JGR Space Physics

RESEARCH ARTICLE
10.1029/2021JA029577

Evolution of IMF B_y Induced Asymmetries: The Role of Tail Reconnection

A. Ohma[1], N. Østgaard[1], K. M. Laundal[1], J. P. Reistad[1], S. M. Hatch[1], and P. Tenfjord[2]

[1]Birkeland Centre for Space Science, University of Bergen, Bergen, Norway, [2]Space Plasma Physics Group, University of Bergen, Bergen, Norway

Key Points:

- The evolution of the asymmetric state of the magnetosphere is examined by using the Lyon-Fedder-Mobarry model with non-zero interplanetary magnetic field B_y
- The simulation shows a clear reduction of north-south asymmetries associated with enhanced tail reconnection
- The modeling results are consistent with the evolution seen in interhemispheric observations of aurora

Correspondence to:
A. Ohma,
anders.ohma@uib.no

Citation:
Ohma, A., Østgaard, N., Laundal, K. M., Reistad, J. P., Hatch, S. M., & Tenfjord, P. (2021). Evolution of IMF B_y induced asymmetries: The role of tail reconnection. *Journal of Geophysical Research: Space Physics*, *126*, e2021JA029577. https://doi.org/10.1029/2021JA029577

Received 18 MAY 2021
Accepted 24 JUN 2021

Abstract North-south asymmetries arise in the magnetosphere-ionosphere system when a significant east-west (B_y) component is present in the interplanetary magnetic field (IMF). During such conditions, a B_y component with the same sign as the IMF B_y component is induced in the magnetosphere, and the locations of conjugate magnetic footpoints are displaced between the two hemispheres. It has been suggested that these asymmetries are introduced into the closed magnetosphere by tail reconnection. However, recent studies instead suggest that asymmetric lobe pressure induces the asymmetries, which are then reduced during periods of enhanced tail reconnection. To address this, we use the Lyon-Fedder-Mobarry (LFM) model and initiate a loading-unloading cycle in multiple runs by changing the IMF. Asymmetries are induced during the loading phase and reduced during the unloading phase. The model results thus suggest that asymmetries arise during periods with low tail reconnection and are reduced during periods with enhanced tail reconnection.

Plain Language Summary The aurora is a bright and beautiful manifestation of Earth's connection to space, and can light up the night sky in the high latitude regions in both hemispheres. However, auroral features do not always occur at the expected magnetic location in the two hemispheres, but are often displaced in the longitudinal direction between the Northern and Southern Hemisphere. The displacement is related to the orientation of the magnetic field in the solar wind, but the exact mechanisms responsible for causing and removing this displacement are debated. Previous simulations of the plasma environment around the Earth suggest that when this magnetic field intensifies in the dawn-dusk direction, magnetic pressure builds up asymmetrically in each hemisphere, causing the displacement. Here we present new simulation results showing that the longitudinal displacement is reduced when magnetic reconnection happens in the Earth's magnetotail.

1. Introduction

North-south asymmetries arise in the magnetosphere-ionosphere system when the interplanetary magnetic field (IMF) has a non-zero east-west (B_y) component. One aspect of these interhemispheric asymmetries is a relative displacement of the ionospheric footpoints of closed magnetic field lines. The displacement is observed in simultaneous images of conjugate auroral features (Frank & Sigwarth, 2003; Østgaard, Mende, Frey, Immel, et al., 2004; Østgaard, Tsyganenko, et al., 2005; Reistad, Østgaard, Laundal, & Oksavik, 2013; Reistad, Østgaard, Tenfjord, et al., 2016) and in the average location of substorm onset (Liou & Newell, 2010; Liou et al., 2001; Østgaard, Mende, Frey, Sigwarth, et al., 2007; Østgaard, Laundal, et al., 2011; Wang et al., 2007), and is associated with a B_y component inside the closed magnetosphere having the same sign as the IMF B_y (Cao et al., 2014; Case et al., 2021; Cowley & Hughes, 1983; Fairfield, 1979; Kaymaz et al., 1994; Petrukovich et al., 2005; Wing et al., 1995). Some studies have suggested that the B_y component induced in the closed magnetosphere is introduced by tail reconnection (Browett et al., 2017; Cowley, 1981; Motoba, Hosokawa, Sato, et al., 2010; Østgaard, Mende, Frey, Immel, et al., 2004; Stenbaek-Nielsen & Otto, 1997), while others have pointed to the build up of an asymmetric pressure distribution in the lobes for non-zero IMF B_y playing the primary role (Khurana et al., 1996; Liou & Newell, 2010; Østgaard, Reistad, et al., 2018; Tenfjord, Østgaard, Haaland, et al., 2018; Tenfjord, Østgaard, Snekvik, et al., 2015; Tenfjord, Østgaard, Strangeway, et al., 2017).

Using global magnetohydrodynamic (MHD) models and observations at geosynchronous orbit, Tenfjord, Østgaard, Snekvik, et al. (2015), Tenfjord, Østgaard, Strangeway, et al. (2017), and Tenfjord, Østgaard, Haaland, et al. (2018) demonstrated that the magnetic field in the closed magnetosphere responds to changes in IMF B_y within about 10 min, and reconfigures to the new orientation within an hour. Similar response and reconfiguration times were found for both northward and southward IMF, on both the dayside and the nightside, and for both polarities of IMF B_y. This prompt response is consistent with asymmetric lobe pressure influencing the closed magnetosphere directly. These results stand in contrast to several studies reporting longer time scales, apparently consistent with asymmetries being introduced by tail reconnection (Browett et al., 2017; Motoba, Hosokawa, Ogawa, et al., 2011; Motoba, Hosokawa, Sato, et al., 2010; Rong et al., 2015). However, Tenfjord, Østgaard, Strangeway, et al. (2017) argued that the magnetic signatures observed in the events analyzed by Motoba, Hosokawa, Ogawa, et al. (2011) and Rong et al. (2015) are not linked to IMF B_y. They stated that the signature observed by Motoba, Hosokawa, Ogawa, et al. (2011) is most likely a bursty bulk flow (Baumjohann et al., 1990), whereas the signatures observed by Rong et al. (2015) are heavily influenced by pressure jumps in the IMF. Furthermore, although Browett et al. (2017) reported delays between IMF B_y and magnetotail B_y of 2–5 h, they focused on the timescales over which the coupling efficiency (fraction of IMF B_y in the magnetosphere) maximizes, and paid less attention to the correlation coefficient.

As pointed out by Ohma, Østgaard, Reistad, Tenfjord, Laundal, Snekvik, et al. (2018), the reported correlations have a different time dependence than the coupling efficiency. For instance, for fast solar wind flows the correlation maximizes for delays of less than one hour for both northward and southward IMF. The peaks in the correlation are also generally broad, making precise determination of the delay difficult. Additionally, as discussed by Ohma, Østgaard, Reistad, Tenfjord, Laundal, Snekvik, et al. (2018), it is unclear how to interpret a linear correlation between the IMF and magnetotail field, given the nonlinear response to changes in IMF B_y observed in the closed magnetosphere (Tenfjord, Østgaard, Haaland, et al., 2018; Tenfjord, Østgaard, Strangeway, et al., 2017). Last, Tenfjord, Østgaard, Haaland, et al. (2018) described how the dependence between IMF B_y and the induced B_y is not necessarily linear after the reconfiguration either, but scales as a coupling function (i.e., is dependent on upstream solar wind parameters such as solar wind speed and IMF magnitude and orientation). The results presented by Browett et al. (2017) are therefore challenging to interpret. In that regard, the results presented by Tenfjord, Østgaard, Snekvik, et al. (2015), Tenfjord, Østgaard, Strangeway, et al. (2017), and Tenfjord, Østgaard, Haaland, et al. (2018) yield response and reconfiguration times in a more straightforward way, and is based on a solid methodology.

Reconnection in the near-Earth tail maximizes during a magnetospheric substorm, a process in which magnetic flux and energy stored in the magnetotail lobes are unloaded explosively (Hones, 1979; Milan et al., 2007). Superposed epoch studies relative to substorm onset have revealed that the magnetic energy and flux stored in the lobes increase in the hours leading up to onset and decrease during the unloading phase following onset (Caan et al., 1975, 1978; Coxon et al., 2018; Yamaguchi et al., 2004). This loading phase prior to onset is associated with increased dayside reconnection and flux transport (Caan et al., 1977; Wild et al., 2009), and regularly referred to as the growth phase (McPherron, 1970). The unloading phase, when the closure of magnetic flux by tail reconnection maximizes, is also referred to as the expansion phase.

Studies that investigate the spatial evolution of conjugate auroral features during substorms have revealed that asymmetries at onset are reduced or even removed during the expansion phase (Østgaard, Humberset, & Laundal, 2011; Østgaard, Reistad, et al., 2018; Ohma, Østgaard, Reistad, Tenfjord, Laundal, Snekvik, et al., 2018). These results suggest that enhanced reconnection in the near-Earth tail acts to reduce the asymmetries induced by the IMF B_y, and Ohma, Østgaard, Reistad, Tenfjord, Laundal, Snekvik, et al. (2018) found a clear relation between the tail reconnection rate and the rate of change of the asymmetries. These observations thus oppose the view that tail reconnection introduces the asymmetries in the closed magnetosphere. However, events with sufficient conjugate coverage are sparse. Saita et al. (2011) examined the relative displacement of conjugate points in a numerical MHD simulation with IMF $B_y \neq 0$ during substorm-like events. While they focus on a large, 1-min displacement occurring at onset, which could be associated with a bursty bulk flow, they also consider the time history of the displacement at a few locations. In their run with negative IMF B_y, the displacement at high latitude locations increases gradually prior to onset and is clearly reduced after onset. The displacement found in the run with positive IMF B_y is more ambiguous, but

a small reduction of the displacement is observed between 25 and 45 min after onset. However, since only a few locations in the magnetotail are considered, the full global response is not explored and their findings could be very localized.

IMF B_y induced asymmetries are also manifested in the ionospheric convection pattern. For positive IMF B_y, a round convection cell forms in the dusk sector in the Northern Hemisphere and in the dawn sector in the Southern Hemisphere, whereas a crescent convection cell forms in the dawn sector in the Northern Hemisphere and in the dusk sector in the Southern Hemisphere (e.g., Haaland et al., 2007; Ruohoniemi & Greenwald, 1995; Thomas & Shepherd, 2018; Weimer, 1995). For negative IMF B_y, the location of the round and crescent convection cells switch place. Recent studies have demonstrated that also the convection in the magnetosphere-ionosphere system is more symmetric for increased activity. Grocott, Milan, et al. (2010) used simultaneous measurements of the ionospheric convection in both hemispheres relative to substorm onset, and demonstrated reduced IMF control and more north-south symmetric convection during the substorm. Further, Reistad, Østgaard, Laundal, Ohma, et al. (2018) showed that the average convection in the closed field line region on the nightside in the Northern Hemisphere became more similar, both in location and magnitude, for positive and negative IMF B_y during intervals with enhanced tail activity.

In the present study, we use a global MHD model to further investigate how increased tail reconnection affects the evolution of the asymmetric state of the magnetosphere. We will also use the modeling results to explore what processes that give rise to the asymmetries in the magnetosphere-ionosphere system. In the following section, we introduce the model used in this study and describe model setup. Further, we describe the methods used to analyze the model data. The results of the simulation is shown in Section 3 and we discuss these results in Section 4. Section 5 concludes the paper.

2. Simulation Setup

The simulations in this study are performed using the coupled-magnetosphere-ionosphere-thermosphere (CMIT) model through the run-on-request service provided by the Community Coordinated Modeling Center (CCMC). The magnetospheric part of the CMIT model is the Lyon-Fedder-Mobarry (LFM) model (Lyon, Fedder, & Mobarry, 2004), which solves the ideal MHD equations to model the solar wind-magnetosphere interaction. The LFM model is coupled to the Magnetosphere-Ionosphere Coupler/solver (MIX) (Merkin & Lyon, 2010), which provides the electrostatic potential at the ionospheric boundary of the LFM model. MIX is further coupled to the Thermosphere Ionosphere Electrodynamics General Circulation model (Richmond et al., 1992). The runs used in this study are available as Anders_Ohma_082219_1, Anders_Ohma_110320_1, and Anders_Ohma_110320_2 at CCMC's run-on-request system and are referred to as Run I, Run II, and Run III, respectively.

Gordeev et al. (2017) examined the response of three commonly used global MHD models to southward turnings of the IMF, and found that only the LFM model had a loading phase followed by an unloading phase, whereas the BATS-R-US and openGGCM model showed a more gradual transition to a new quasi-equilibrium. The CMIT/LFM-MIX global MHD model is therefore well suited to address how enhanced near-Earth tail reconnection affects the asymmetric state of the magnetosphere. In Run I, we apply the same strategy as used by Gordeev et al. (2017) to trigger a loading-unloading cycle in the simulation; a polarity change of the IMF B_z component. IMF B_z is 1 h of -5 nT, then 2 h of 5 nT, and finally 2 h of -5 nT, while IMF B_y is kept constant at -5 nT throughout the run. Zero epoch time is set at the southward turning of the IMF 3 h into the run. The southward turning increases the dayside reconnection rate Φ_D and the magnetic flux transport, which will eventually trigger enhanced nightside, or tail, reconnection rate Φ_N. Having run the simulation with IMF $B_y = -5$ nT for three hours prior the southward turning, we ensure that the induced B_y and associated north-south asymmetries are established in the simulation before the loading-unloading cycle. In Run II and Run III, we employ a different strategy to initiate a loading-unloading cycle. Instead of changing the IMF B_z component, we initiate a loading-unloading cycle by introducing a large IMF B_y component while keeping the IMF B_z component at a small constant level. IMF B_z is kept constant at 1 nT in Run II (northward IMF) and at -1 nT in Run III (southward IMF). In both runs, IMF B_y is zero for 1 h then 10 nT for 2 h. The small IMF B_z during the first hour ensures that Φ_D is low (although higher

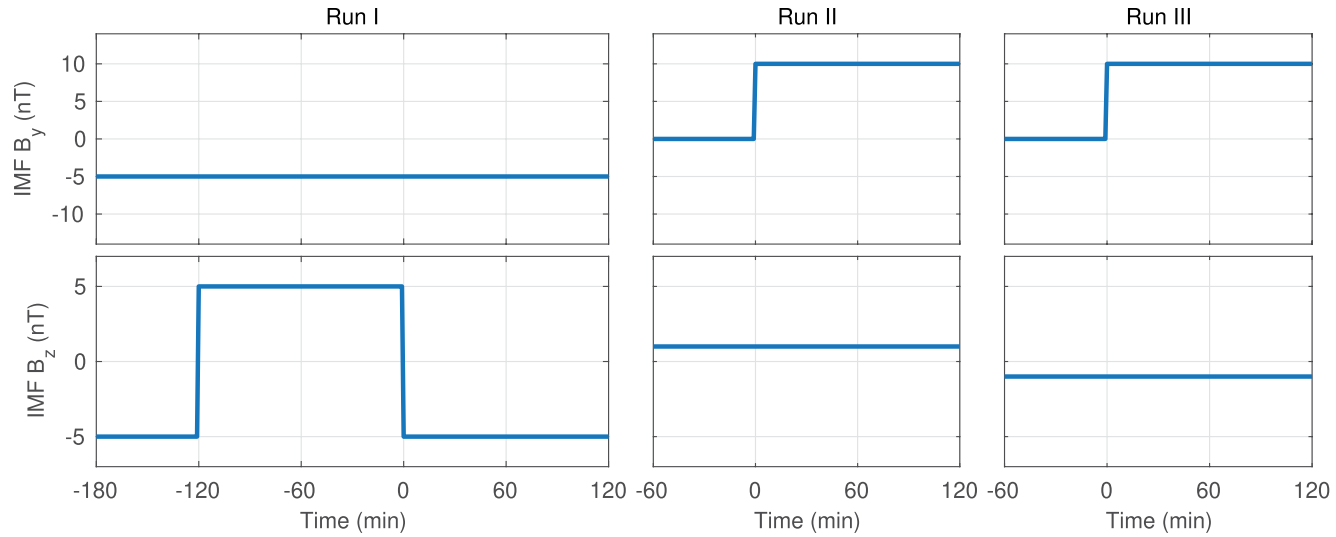

Figure 1. IMF input values for the three different runs.

for IMF $B_z = -1$ nT than for IMF $B_z = +1$ nT), which means that Φ_D increases significantly when IMF B_y is introduced in the simulation. Zero epoch is set when the IMF B_y component is introduced.

In Run I, the IMF B_y induced asymmetries are present at the start of the loading-unloading cycle, whereas the asymmetries are introduced during the loading phase in Run II and Run III, from a northward and southward configuration, respectively. The three runs thus represent three different initial configurations at the start of the loading-unloading cycle. The IMF input used in the three model runs are shown in Figure 1. The other simulation parameters are equal and constant in all runs: Radial solar wind with velocity of 400 km/s, density of 5 cm^{-3} and temperature of 200,000 K, solar radio flux at 10.7 cm (F10.7) of 150 sfu, IMF $B_x = 0$, grid resolution of $106 \times 96 \times 128$ cells and auroral conductance. In order to isolate the influence of IMF B_y on the magnetosphere, all three runs have no dipole tilt. However, we note that non-zero dipole tilt is expected to affect the asymmetric state of the magnetosphere due to for example, different exposure of the two hemispheres to the solar wind, interhemispheric differences in the lobe reconnection rate (Crooker & Rich, 1993; Reistad, Laundal, et al., 2019) and warping of the magnetotail neutral sheet (Liou & Newell, 2010; Petrukovich, 2009; Tsyganenko & Fairfield, 2004).

In order to get quantitative information about the evolution of the magnetospheric configuration during the loading-unloading cycle, we extract several key parameters from the model runs. The amount of open flux in the polar cap F_{PC} is available from CCMC as a pre-calculated output. As demanded by the expanding/contracting polar cap paradigm (Cowley & Lockwood, 1992; Siscoe & Huang, 1985), changes in F_{PC} are given as $dF_{\mathrm{PC}}/dt = \Phi_D - \Phi_N$. F_{PC} increases when $\Phi_D > \Phi_N$ (expanding polar cap, loading phase) and decreases when $\Phi_D < \Phi_N$ (contracting polar cap, unloading phase). To get other relevant state parameters, we consider a cross-section of the magnetosphere at $X_{\mathrm{SM}} = -12\ R_E$ in Solar Magnetic (SM) Coordinates, as shown in Figure 2a, similar to the approach employed by Gordeev et al. (2017). Note that SM coordinates are equivalent to Geocentric Solar Magnetic (GSM) Coordinates since there is no dipole tilt in the simulations. We identify the magnetopause in this cross-section by assuming that the mass flux inside the magnetopause is 0.3 times the background solar wind mass flux, as suggested by Peng et al. (2010). This is a simple and robust way to determine the magnetopause, and yields a location that is, consistent with the location determined by other methods (Gordeev et al., 2017; Palmroth et al., 2003). The open-closed boundary (OCB) is identified by field line tracing. The regions between the magnetopause and OCB in each hemisphere is used to calculate the magnetic pressure P_L in the two lobes. In order to quantify the amount of flux that is, transported toward the Earth in the tail, we estimate the cross-tail potential (CTP). Similar to Gordeev et al. (2017), we estimate this quantity as $\mathrm{CTP} = -\int \left(\mathbf{V} \times \mathbf{B}\right)_y dy$, integrating along the Y_{SM} axis in the equatorial plane from -15 to $+15\ R_E$. $\mathbf{V}$ and $\mathbf{B}$ are the plasma velocity and the magnetic field, respectively. $-\mathbf{V} \times \mathbf{B}$ quantifies magnetic flux transport and is displayed as white vectors in Figure 2a. The CTP is thus an integral measure of the magnetic flux

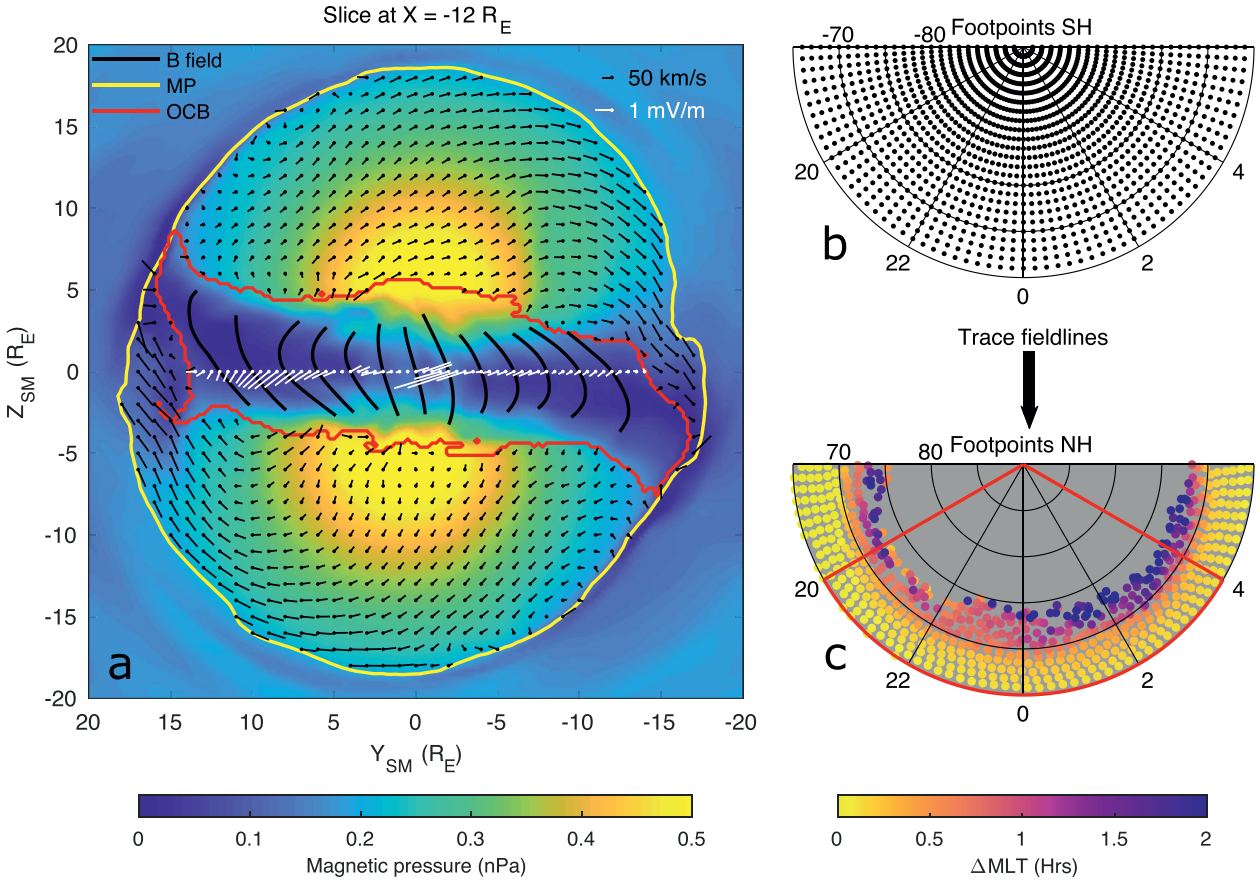

Figure 2. (a) Cross-section of the magnetosphere at $X_{SM} = -12\ R_E$ at $t = 40$ min in Run III. The black vectors display the convection in the two lobes and the white vectors the convection electric field along $Z_{SM} = 0$. The background colors indicate the magnetic pressure, whereas the magnetopause and OCB are indicated by magenta and red, respectively. The black lines show the magnetic field lines crossing the equatorial plane at $X_{SM} = -12\ R_E$ with 2-R_E spacing. (b) Grid of ionospheric footpoints in the Southern Hemisphere. (c) Location of the conjugate footpoints in the Northern Hemisphere. The colors indicate the relative longitudinal displacement measured in hours.

transport in the equatorial plane at $X_{SM} = -12\ R_E$, and is insensitive to the location of the reconnection line in the tail (Gordeev et al., 2017). We also calculate the average B_y component along the same line.

To quantify the relative displacement of conjugate regions, we trace a set of points from the southern to the northern ionosphere along the magnetic field. The initial grid is shown in Figure 2b and the location of the mapped footpoints are displayed in Figure 2c during a time with positive IMF B_y. The color indicates the relative displacement in the longitudinal direction between the hemispheres, defined as $\Delta\text{MLT} = \text{MLT}_{\text{south}} - \text{MLT}_{\text{north}}$. Positive values thus mean that the northern footpoint is earlier in magnetic local time (MLT) than the southern footpoint. In order to get a single global value of the displacement at each time step, we calculate the average displacement between 20 and 4 MLT, indicated by the red segment. We note that the results reported in the next section are not sensitive to the exact size of this region. An advantage of this quantity is that it represents the global asymmetry of the magnetosphere, not just at a specific location in the magnetosphere.

3. Results

The global response of the magnetosphere in the three runs is displayed in Figure 3. The first row shows the evolution of open flux F_{PC} and the second row the evolution of lobe pressure P_L at $X_{SM} = -12\ R_E$. The third and fourth row display the CTP and the absolute value of the induced B_y, respectively, estimated as described in the previous section. The thin lines display the instantaneous values and the thick lines display the 5-min running average. Finally, the fifth row shows the average |ΔMLT| (absolute value). By examining

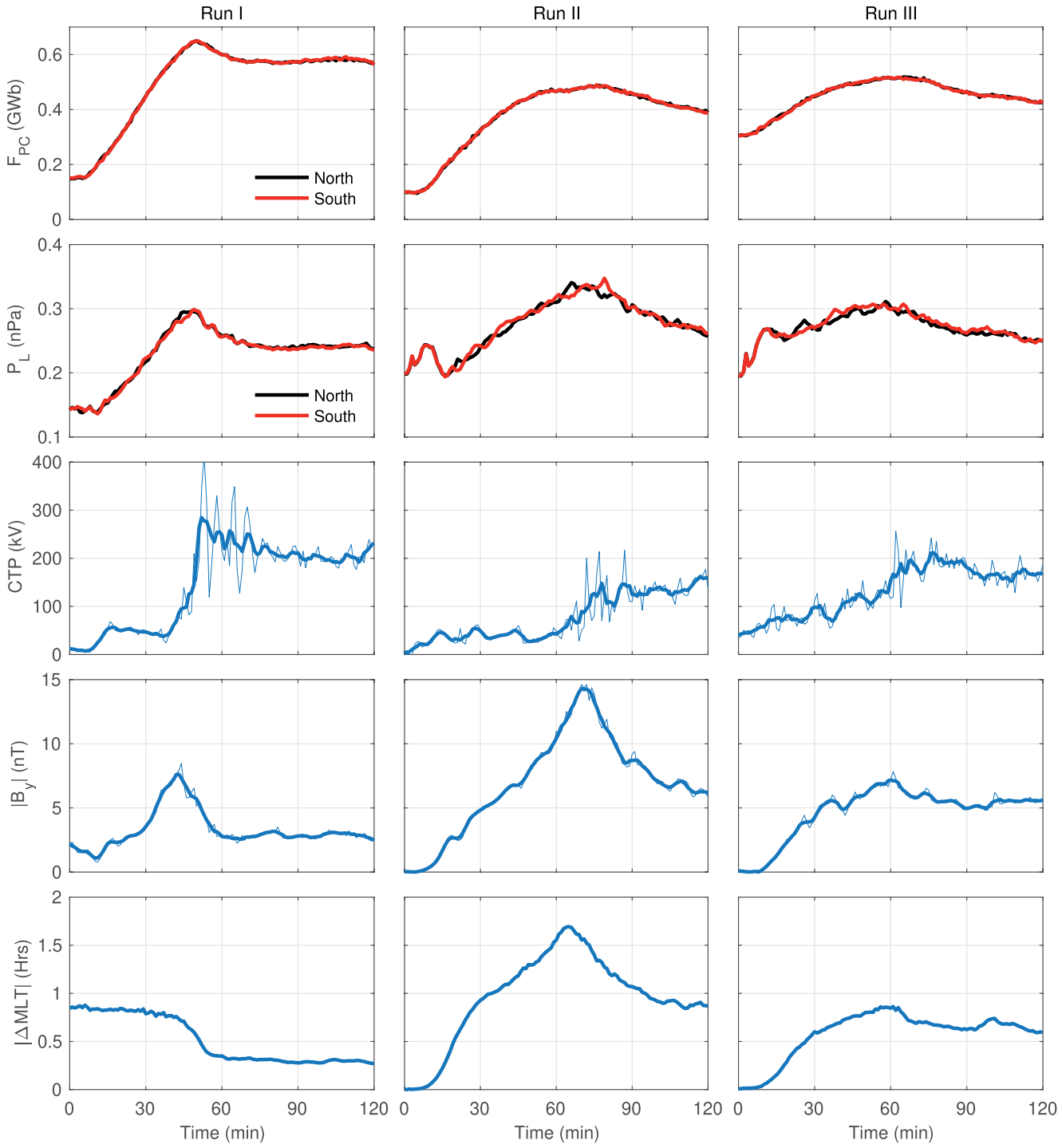

Figure 3. Global output parameters from the three runs. Each column correspond to a different run. From the top; Amount of open magnetic flux in both hemispheres, magnetic pressure in both lobes, CTP at $X_{SM} = -12\ R_E$, absolute value of the average induced B_y at $X_{SM} = -12\ R_E$ and absolute value of the average longitudinal displacement between the two hemispheres.

the two upper rows in the figure, it is clear that the imposed changes in the IMF at zero epoch have indeed initiated a loading-unloading cycle in all runs.

In Run I, F_{PC} and P_L start to increase about 10 min after the southward turning of the IMF, consistent with the IMF travel time from the bow shock. Both quantities maximize after about 50 min, followed by

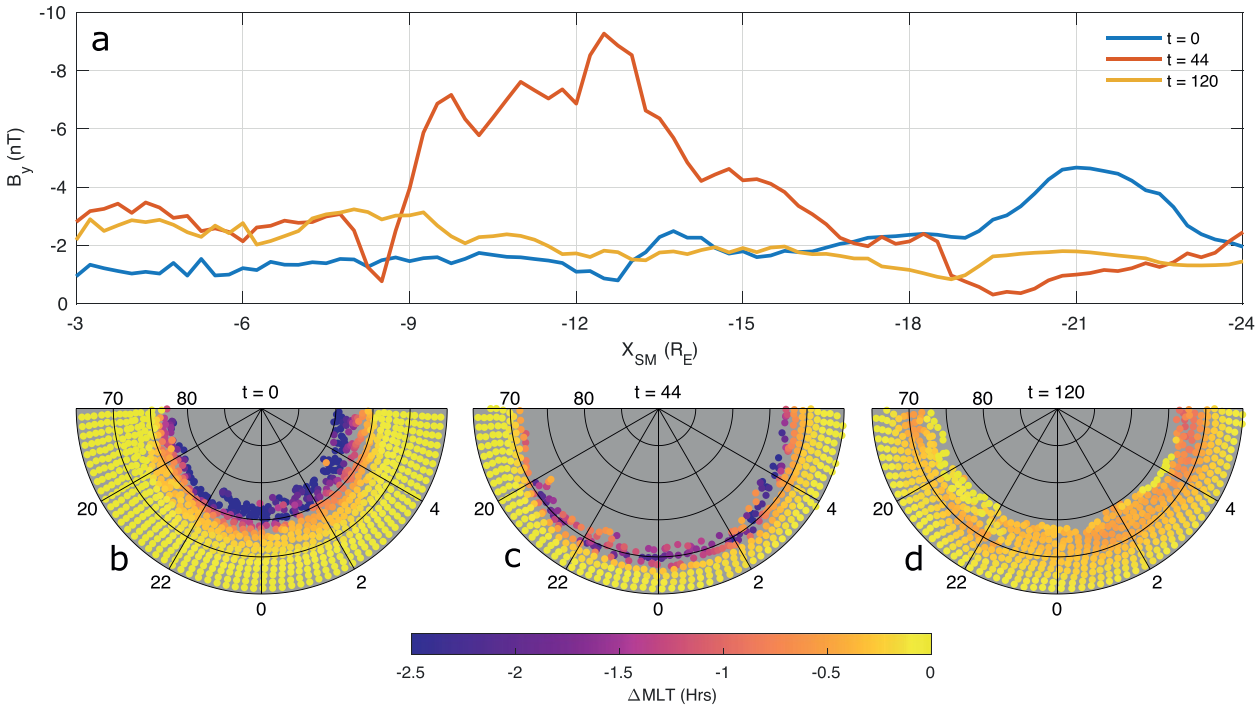

Figure 4. (a) B_y along the X_{SM} axis at $t = 0$ (blue), $t = 44$ (red), and $t = 120$ (amber). (b) Relative displacement at $t = 0$. (c) Relative displacement at $t = 44$. (d) Relative displacement at $t = 120$.

a decrease for about 20 min before they stabilize. The unloading is associated with a rapid increase in the CTP, which indicates a significant enhancement of Φ_N. From the two lower panels, it is clear that both $|B_y|$ and |ΔMLT| decrease rapidly when the enhanced tail reconnection commences. After the unloading, $\Phi_D \approx \Phi_N$, and the asymmetries remain constant. The evolution of $|B_y|$ and |ΔMLT| during the loading phase display interesting differences: While |ΔMLT| is relatively stable during the loading phase, the average $|B_y|$ at $X_{SM} = -12\ R_E$ increases during this phase. The reason they behave differently is that the initial asymmetry occurs at higher latitudes in the ionosphere, corresponding to farther tailward in the magnetosphere, and is not observed at this location before the OCB have expanded significantly. This behavior is investigated separately below (Figure 4).

The global response of Run II is shown in the second column of the figure. The initial value of F_{PC} at $t = 0$ min is slightly lower compared to the first run, a consequence of the purely northward IMF in the preceding hour. F_{PC} starts to increase within 10 min, which means that IMF B_y leads to enhanced dayside reconnection. Again, F_{PC} and P_L follow a similar evolution. Both quantities maximize at around $t = 75$ min, followed by a decrease for the rest of the simulation. This decrease is associated with a significant increase in the CTP and implies that $\Phi_N > \Phi_D$. As evident from the two lower panels, north-south asymmetries arise as soon as F_{PC} and P_L start to increase, and the magnetosphere continues to become more asymmetric during the loading phase. Both the induced B_y and average longitudinal displacement maximize near the onset of the unloading phase. Both quantities then rapidly decrease, which indicates that the increased Φ_N reduces the asymmetric state of the magnetosphere.

Run III has a similar setup as Run II, except that it starts from a southward configuration. Hence, the initial value of F_{PC} is greater in this run compared to Runs I and II. After the IMF B_y component is introduced, both F_{PC} and P_L start to increase. However, the rate of increase is small compared to the other runs, indicating a more balanced Φ_D and Φ_N. This is supported by the CTP, which is considerably higher during the loading phase in this run compared to Run II. Also in this run, the initial response in both the induced B_y and ΔMLT occurs after only 10 min, and the asymmetries increase throughout the loading phase ($\Phi_D > \Phi_N$). Again, the asymmetries maximize near the onset of the unloading phase, and are reduced during the unloading phase, albeit less pronounced than in the other two runs.

The different evolution of the induced B_y and ΔMLT during the loading phase in Run I is addressed in Figure 4. The induced B_y in the closed magnetotail along the X_{SM} axis is displayed in Figure 4a. The blue curve is at $t = 0$ min (succeeding 2 h of northward IMF), the red curve is at $t = 44$ min (maximum B_y at $X_{SM} = -12\ R_E$) and the amber curve is at $t = 120$ min (succeeding 2 h of southward IMF). Figures 4b–4d show the relative displacement at the three time steps. The magnetosphere is clearly asymmetric at $t = 0$, but the foopoints with large ΔMLT are mainly above 73° magnetic latitude. Correspondingly, B_y peaks at $X_{SM} = -21\ R_E$, but is only 1–2 nT for $X_{SM} > -19\ R_E$. At $t = 44$, the polar cap has expanded due to the enhanced Φ_D, and the asymmetries are at lower latitudes. This is reflected in the induced B_y component as a broad peak between −9 and −18 R_E. The increase in B_y observed at $X_{SM} = -12\ R_E$ during the loading phase is thus a result of the OCB expanding, moving the most asymmetric region closer to Earth. Figure 4d displays ΔMLT when the magnetosphere has reached a new quasi-equilibrium following the unloading phase. The magnetosphere is clearly more symmetric near the OCB compared to the two other time steps. However, B_y is actually higher within $-13\ R_E$, compared to $t = 0$.

4. Discussion

The simulations presented above show how the large scale asymmetric state of the magnetosphere evolves during a loading-unloading cycle. In Runs II and III, the loading phase is initiated by introducing a large IMF B_y component from a symmetric configuration. The magnetosphere becomes increasingly asymmetric during the loading phase when $\Phi_D > \Phi_N$, and maximize near the onset of increased Φ_N. In Run II, the north-south asymmetries are clearly reduced during the unloading phase. Compared to Run II, the asymmetries appear more slowly in Run III, and the reduction of north-south asymmetries during the unloading phase is less pronounced. When considering the more balanced Φ_D and Φ_N in this run, this is the expected behavior: The CTP, and thus Φ_N, is significantly higher during the loading phase in this run, prohibiting a fast build up of lobe pressure. In Run I, asymmetries are already present at $t = 0$ min, as the preceding 3-h interval also contains the same IMF B_y component. A clear reduction of the north-south asymmetries is observed when $\Phi_N > \Phi_D$ also in this run.

The presented results are consistent with ionospheric observations of plasma convection and conjugate auroral features, both suggesting reduced asymmetry for enhanced near-Earth tail reconnection during substorm expansion phase (Grocott, Milan, et al., 2010; Ohma, Østgaard, Reistad, Tenfjord, Laundal, Snekvik, et al., 2018; Østgaard, Laundal, et al., 2011; Østgaard, Reistad, et al., 2018; Reistad, Østgaard, Laundal, Ohma, et al., 2018). They are also consistent with the modeling results presented by Saita et al. (2011), in particular their run with negative IMF B_y. It has been proposed by for example, Østgaard, Reistad, et al. (2018) that the reduction is directly linked to the reduction of lobe pressure when $\Phi_N > \Phi_D$, as this asymmetric lobe pressure is presumed to be the source of the initial asymmetry (Khurana et al., 1996; Tenfjord, Østgaard, Snekvik, et al., 2015). However, the auroral observations suggest that the asymmetries can be almost entirely removed, which is not seen in the simulations. Here it is worth noting that the loading-unloading cycles initiated in the runs only mimic substorm behavior, they are not completely similar. Juusola et al. (2011) showed that the frequency of bursty bulk flows, which are strongly linked to the tail reconnection rate, continue to increase rapidly during the expansion phase and maximize at the beginning of the recovery phase. While the tail reconnection in the simulations reported here do increase enough to reduce the F_{PC} significantly, Φ_N does not continue to increase explosively. In that regard, the simulations appear to go into a quasi-equilibrium, and are thus more similar to steady magnetospheric convection events (Sergeev et al., 1996). On the same note, Milan et al. (2007) found that substorms typically close about 0.3 GWb of open flux, whereas only ∼0.1 GWb is closed in the runs presented here. Such differences are expected, as ideal MHD models rely on anomalous resistivity to mimic the reconnection process. The LFM model relies on numerical diffusion to allow for reconnection, resulting from the finite volume techniques used to solve the MHD equations (Lyon, Fedder, & Mobarry, 2004). Other implementations of reconnection in ideal MHD models exist, and differences between implementations on magnetotail dynamics are discussed by for example, Lyon, Fedder, and Huba (1986). However, the model is expected to properly capture how the surrounding configuration of the magnetosphere responds to changes in Φ_D and Φ_N in a self-consistent way, regardless of the exact implementation of the reconnection process. The presented results should therefore

not be affected by this, as long as the implemented anomalous resistivity allows for loading-unloading cycles in the simulation.

The model runs show a reduction of the asymmetries when $\Phi_N > \Phi_D$ and thus contradict the studies suggesting that IMF B_y and associated north-south asymmetries are introduced into the closed magnetosphere by tail reconnection (e.g., Browett et al., 2017; Motoba, Hosokawa, Ogawa, et al., 2011; Rong et al., 2015). As noted in the introduction, the interpretation of some of these observations is disputed (Ohma, Østgaard, Reistad, Tenfjord, Laundal, Snekvik, et al., 2018; Tenfjord, Østgaard, Strangeway, et al., 2017). It is also worth noting that these studies only base their conclusion on the inferred time lags between IMF B_y and the induced B_y, and do not consider measurements, directly or indirectly, of Φ_N. Contrarily, Φ_N is accounted for in this analysis and in the analysis performed by Ohma, Østgaard, Reistad, Tenfjord, Laundal, Snekvik, et al. (2018) by considering changes in F_{PC} (and CTP), and the relationship between Φ_N and the asymmetric state of the magnetosphere is thus addressed more directly.

Several studies have shown that the coupling efficiency between IMF B_y and the induced B_y in the inner magnetosphere is higher for southward compared to northward IMF (e.g., Case et al., 2021; Tenfjord, Østgaard, Haaland, et al., 2018; Tenfjord, Østgaard, Strangeway, et al., 2017). Consistent results are seen in Run I, where the induced B_y earthward of -13 R_E is higher at $t = 120$ compared to $t = 0$. Case et al. (2021) argued that this dependence indicates that tail reconnection induces the B_y component, since periods with enhanced Φ_N occur more frequently during southward IMF. However, as evident from Figures 4b and 4d, the magnetosphere is generally more asymmetric at $t = 0$ compared to $t = 120$, the asymmetry is just located farther poleward in the ionosphere, that is, farther tailward in the magnetosphere. Larger north-south asymmetries for northward IMF compared to southward IMF is also consistent with both ionospheric and magnetospheric observations of plasma convection (Grocott & Milan, 2014; Grocott, Yeoman, et al., 2005; Ohma, Østgaard, Reistad, Tenfjord, Laundal, Moretto Jørgensen, et al., 2019). A more likely explanation of the higher coupling efficiency is therefore that these regions are much closer to the OCB during southward IMF, which makes the induced B_y larger in the inner magnetosphere although the magnetosphere is globally less asymmetric.

5. Summary

By analyzing three different runs of the LFM model, we have demonstrated that the B_y component in the magnetotail and north-south displacement of conjugate magnetic footpoints are reduced by enhanced tail reconnection. In Run I, where the simulation setup ensured an asymmetric configuration at the start of the loading-unloading cycle, the asymmetries persist until the tail reconnection rate increases during the unloading phase. In Runs II and III, which were symmetric when the loading-unloading cycle was initiated, the asymmetries continues to increase during the loading phase, maximizes near the onset of the unloading phase and are reduced during the unloading of the lobes. These results are inconsistent with tail reconnection introducing the IMF B_y component, and hence the asymmetries, into the closed magnetosphere, but are consistent with the asymmetries being introduced by pressure gradients in the magnetotail lobes. The results are further supported by conjugate observations of aurora and convection. Hence, we conclude that the asymmetric loading of magnetic flux in the two lobes directly influences the asymmetric state of the magnetosphere, and that the relaxation of the magnetosphere from an excited state that occurs during a substorm also acts to return the north-south asymmetries toward a more symmetric configuration.

Data Availability Statement

Simulation results have been provided by the Community Coordinated Modeling Center at Goddard Space Flight Center through their public Runs-on-Request system (http://ccmc.gsfc.nasa.gov).

Acknowledgments
This study was supported by the Research Council of Norway/CoE under contract 223252/F50. P. Tenfjord received support from the Research Council of Norway under contract 300865. J. P. Reistad was funded by the Norwegian Research Council through grant 300844/F50.

References

Baumjohann, W., Paschmann, G., & Lühr, H. (1990). Characteristics of high-speed ion flows in the plasma sheet. *Journal of Geophysical Research: Space Physics*, *95*(A4), 3801–3809. https://doi.org/10.1029/JA095iA04p03801

Browett, S. D., Fear, R. C., Grocott, A., & Milan, S. E. (2017). Timescales for the penetration of IMF B_y into the Earth's magnetotail. *Journal of Geophysical Research: Space Physics*, *122*(1), 579–593. https://doi.org/10.1002/2016JA023198

Caan, M. N., McPherron, R. L., & Russell, C. T. (1975). Substorm and interplanetary magnetic field effects on the geomagnetic tail lobes. *Journal of Geophysical Research*, *80*(1), 191–194. https://doi.org/10.1029/JA080i001p00191

Caan, M. N., McPherron, R. L., & Russell, C. T. (1977). Characteristics of the association between the interplanetary magnetic field and substorms. *Journal of Geophysical Research*, *82*(29), 4837–4842. https://doi.org/10.1029/JA082i029p04837

Caan, M. N., McPherron, R. L., & Russell, C. T. (1978). The statistical magnetic signature of magnetospheric substorms. *Planetary and Space Science*, *26*(3), 269–279. https://doi.org/10.1016/0032-0633(78)90092-2

Cao, J., Duan, A., Dunlop, M. W., Wei, X., & Cai, C. (2014). Dependence of IMF B_y penetration into the neutral sheet on IMF B_z and geomagnetic activity. *Journal of Geophysical Research: Space Physics*, *119*(7), 5279–5285. https://doi.org/10.1002/2014JA019827

Case, N. A., Hartley, D. P., Grocott, A., Miyoshi, Y., Matsuoka, A., Imajo, S., et al. (2021). Inner magnetospheric response to the interplanetary magnetic field B_y component: Van Allen Probes and Arase observations. *Journal of Geophysical Research: Space Physics*, *126*(1), e2020JA028765. https://doi.org/10.1029/2020JA028765

Cowley, S. W. H. (1981). Magnetospheric asymmetries associated with the y-component of the IMF. *Planetary and Space Science*, *29*(1), 79–96. https://doi.org/10.1016/0032-0633(81)90141-0

Cowley, S. W. H., & Hughes, W. J. (1983). Observation of an IMF sector effect in the Y magnetic field component at geostationary orbit. *Planetary and Space Science*, *31*(1), 73–90. https://doi.org/10.1016/0032-0633(83)90032-6

Cowley, S. W. H., & Lockwood, M. (1992). Excitation and decay of solar wind-driven flows in the magnetosphere-ionosphere system. *Annales Geophysicae*, *10*(1–2), 103–115.

Coxon, J. C., Freeman, M. P., Jackman, C. M., Forsyth, C., Rae, I. J., & Fear, R. C. (2018). Tailward propagation of magnetic energy density variations with respect to substorm onset times. *Journal of Geophysical Research: Space Physics*, *123*(6), 4741–4754. https://doi.org/10.1029/2017JA025147

Crooker, N. U., & Rich, F. J. (1993). Lobe cell convection as a summer phenomenon. *Journal of Geophysical Research: Space Physics*, *98*(A8), 13403–13407. https://doi.org/10.1029/93JA01037

Fairfield, D. H. (1979). On the average configuration of the geomagnetic tail. *Journal of Geophysical Research: Space Physics*, *84*(A5), 1950–1958. https://doi.org/10.1029/JA084iA05p01950

Frank, L. A., & Sigwarth, J. B. (2003). Simultaneous images of the northern and southern auroras from the Polar spacecraft: An auroral substorm. *Journal of Geophysical Research: Space Physics*, *108*(A4), 8015. https://doi.org/10.1029/2002JA009356

Gordeev, E., Sergeev, V., Tsyganenko, N., Kuznetsova, M., Rastäetter, L., Raeder, J., et al. (2017). The substorm cycle as reproduced by global MHD models. *Space Weather*, *15*(1), 131–149. https://doi.org/10.1002/2016SW001495

Grocott, A., & Milan, S. E. (2014). The influence of IMF clock angle timescales on the morphology of ionospheric convection. *Journal of Geophysical Research: Space Physics*, *119*(7), 5861–5876. https://doi.org/10.1002/2014JA020136

Grocott, A., Milan, S. E., Yeoman, T. K., Sato, N., Yukimatu, A. S., & Wild, J. A. (2010). Superposed epoch analysis of the ionospheric convection evolution during substorms: IMF B_Y dependence. *Journal of Geophysical Research: Space Physics*, *115*(A5), A00105. https://doi.org/10.1029/2010JA015728

Grocott, A., Yeoman, T. K., Milan, S. E., & Cowley, S. W. H. (2005). Interhemispheric observations of the ionospheric signature of tail reconnection during IMF-northward non-substorm intervals. *Annales Geophysicae*, *23*(5), 1763–1770. https://doi.org/10.5194/angeo-23-1763-2005

Haaland, S. E., Paschmann, G., Förster, M., Quinn, J. M., Torbert, R. B., McIlwain, C. E., et al. (2007). High-latitude plasma convection from Cluster EDI measurements: Method and IMF-dependence. *Annales Geophysicae*, *25*(1), 239–253. https://doi.org/10.5194/angeo-25-239-2007

Hones, E. W. (1979). Transient phenomena in the magnetotail and their relation to substorms. *Space Science Reviews*, *23*(3), 393–410. https://doi.org/10.1007/BF00172247

Juusola, L., Østgaard, N., Tanskanen, E., Partamies, N., & Snekvik, K. (2011). Earthward plasma sheet flows during substorm phases. *Journal of Geophysical Research: Space Physics*, *116*(A10), A10228. https://doi.org/10.1029/2011JA016852

Kaymaz, Z., Siscoe, G. L., Luhmann, J. G., Lepping, R. P., & Russell, C. T. (1994). Interplanetary magnetic field control of magnetotail magnetic field geometry: IMP 8 observations. *Journal of Geophysical Research: Space Physics*, *99*(A6), 11113–11126. https://doi.org/10.1029/94JA00300

Khurana, K. K., Walker, R. J., & Ogino, T. (1996). Magnetospheric convection in the presence of interplanetary magnetic field B_y: A conceptual model and simulations. *Journal of Geophysical Research: Space Physics*, *101*(A3), 4907–4916. https://doi.org/10.1029/95JA03673

Liou, K., & Newell, P. T. (2010). On the azimuthal location of auroral breakup: Hemispheric asymmetry. *Geophysical Research Letters*, *37*(23), L23103. https://doi.org/10.1029/2010GL045537

Liou, K., Newell, P. T., Sibeck, D. G., Meng, C.-I., Brittnacher, M., & Parks, G. (2001). Observation of IMF and seasonal effects in the location of auroral substorm onset. *Journal of Geophysical Research: Space Physics*, *106*(A4), 5799–5810. https://doi.org/10.1029/2000JA003001

Lyon, J. G., Fedder, J. A., & Huba, J. D. (1986). The effect of different resistivity models on magnetotail dynamics. *Journal of Geophysical Research: Space Physics*, *91*(A7), 8057–8064. https://doi.org/10.1029/JA091iA07p08057

Lyon, J. G., Fedder, J. A., & Mobarry, C. M. (2004). The Lyon–Fedder–Mobarry (LFM) global MHD magnetospheric simulation code. *Journal of Atmospheric and Solar-Terrestrial Physics*, *66*(15), 1333–1350. (Towards an Integrated Model of the Space Weather System). https://doi.org/10.1016/j.jastp.2004.03.020

McPherron, R. L. (1970). Growth phase of magnetospheric substorms. *Journal of Geophysical Research*, *75*(28), 5592–5599. https://doi.org/10.1029/JA075i028p05592

Merkin, V. G., & Lyon, J. G. (2010). Effects of the low-latitude ionospheric boundary condition on the global magnetosphere. *Journal of Geophysical Research: Space Physics*, *115*(A10), A10202. https://doi.org/10.1029/2010JA015461

Milan, S. E., Provan, G., & Hubert, B. (2007). Magnetic flux transport in the Dungey cycle: A survey of dayside and nightside reconnection rates. *Journal of Geophysical Research: Space Physics*, *112*(1), A01209. https://doi.org/10.1029/2006JA011642

Motoba, T., Hosokawa, K., Ogawa, Y., Sato, N., Kadokura, A., Buchert, S. C., & Rème, H. (2011). In situ evidence for interplanetary magnetic field induced tail twisting associated with relative displacement of conjugate auroral features. *Journal of Geophysical Research: Space Physics*, *116*(4), A04209. https://doi.org/10.1029/2010JA016206

Motoba, T., Hosokawa, K., Sato, N., Kadokura, A., & Bjornsson, G. (2010). Varying interplanetary magnetic field B_y effects on interhemispheric conjugate auroral features during a weak substorm. *Journal of Geophysical Research: Space Physics*, *115*(A9), A09210. https://doi.org/10.1029/2010JA015369

Ohma, A., Østgaard, N., Reistad, J. P., Tenfjord, P., Laundal, K. M., Moretto Jørgensen, T., et al. (2019). Observations of asymmetric lobe convection for weak and strong tail activity. *Journal of Geophysical Research: Space Physics*, *124*(12), 9999–10017. https://doi.org/10.1029/2019JA026773

Ohma, A., Østgaard, N., Reistad, J. P., Tenfjord, P., Laundal, K. M., Snekvik, K., et al. (2018). Evolution of asymmetrically displaced footpoints during substorms. *Journal of Geophysical Research: Space Physics*, *123*. https://doi.org/10.1029/2018JA025869

Østgaard, N., Humberset, B. K., & Laundal, K. M. (2011). Evolution of auroral asymmetries in the conjugate hemispheres during two substorms. *Geophysical Research Letters*, *38*(3), L03101. https://doi.org/10.1029/2010GL046057

Østgaard, N., Laundal, K. M., Juusola, L., Åsnes, A., Haaland, S. E., & Weygand, J. M. (2011). Interhemispherical asymmetry of substorm onset locations and the interplanetary magnetic field. *Geophysical Research Letters*, *38*(8), L08104. https://doi.org/10.1029/2011GL046767

Østgaard, N., Mende, S. B., Frey, H. U., Immel, T. J., Frank, L. A., Sigwarth, J. B., & Stubbs, T. J. (2004). Interplanetary magnetic field control of the location of substorm onset and auroral features in the conjugate hemispheres. *Journal of Geophysical Research: Space Physics*, *109*(A7), A07204. https://doi.org/10.1029/2003JA010370

Østgaard, N., Mende, S. B., Frey, H. U., Sigwarth, J. B., Åsnes, A., & Weygand, J. M. (2007). Auroral conjugacy studies based on global imaging. *Journal of Atmospheric and Solar-Terrestrial Physics*, *69*(3), 249–255. (Global Aspects of Magnetosphere-Ionosphere Coupling). https://doi.org/10.1016/j.jastp.2006.05.026

Østgaard, N., Reistad, J. P., Tenfjord, P., Laundal, K. M., Rexer, T., Haaland, S. E., et al. (2018). The asymmetric geospace as displayed during the geomagnetic storm on 17 August 2001. *Annales Geophysicae*, *36*(6), 1577–1596. https://doi.org/10.5194/angeo-36-1577-2018

Østgaard, N., Tsyganenko, N. A., Mende, S. B., Frey, H. U., Immel, T. J., Fillingim, M., et al. (2005). Observations and model predictions of substorm auroral asymmetries in the conjugate hemispheres. *Geophysical Research Letters*, *32*(5), L05111. https://doi.org/10.1029/2004GL022166

Palmroth, M., Pulkkinen, T. I., Janhunen, P., & Wu, C.-C. (2003). Stormtime energy transfer in global MHD simulation. *Journal of Geophysical Research: Space Physics*, *108*(A1), 1048. https://doi.org/10.1029/2002JA009446

Peng, Z., Wang, C., & Hu, Y. Q. (2010). Role of IMF B_x in the solar wind-magnetosphere-ionosphere coupling. *Journal of Geophysical Research: Space Physics*, *115*(A8), A08224. https://doi.org/10.1029/2010JA015454

Petrukovich, A. A. (2009). Dipole tilt effects in plasma sheet B_y: Statistical model and extreme values. *Annales Geophysicae*, *27*(3), 1343–1352. https://doi.org/10.5194/angeo-27-1343-2009

Petrukovich, A. A., Baumjohann, W., Nakamura, R., Runov, A., & Balogh, A. (2005). Cluster vision of the magnetotail current sheet on a macroscale. *Journal of Geophysical Research: Space Physics*, *110*(A6). https://doi.org/10.1029/2004JA010825

Reistad, J. P., Laundal, K. M., Østgaard, N., Ohma, A., Thomas, E. G., Haaland, S., et al. (2019). Separation and quantification of ionospheric convection sources: 2. The dipole tilt angle influence on reverse convection cells during northward IMF. *Journal of Geophysical Research: Space Physics*, *124*(7), 6182–6194. https://doi.org/10.1029/2019JA026641

Reistad, J. P., Østgaard, N., Laundal, K. M., Ohma, A., Snekvik, K., Tenfjord, P., et al. (2018). Observations of asymmetries in ionospheric return flow during different levels of geomagnetic activity. *Journal of Geophysical Research: Space Physics*, *123*. https://doi.org/10.1029/2017JA025051

Reistad, J. P., Østgaard, N., Laundal, K. M., & Oksavik, K. (2013). On the non-conjugacy of nightside aurora and their generator mechanisms. *Journal of Geophysical Research: Space Physics*, *118*(6), 3394–3406. https://doi.org/10.1002/jgra.50300

Reistad, J. P., Østgaard, N., Tenfjord, P., Laundal, K. M., Snekvik, K., Haaland, S. E., et al. (2016). Dynamic effects of restoring footpoint symmetry on closed magnetic field lines. *Journal of Geophysical Research: Space Physics*, *121*(5), 3963–3977. https://doi.org/10.1002/2015JA022058

Richmond, A. D., Ridley, E. C., & Roble, R. G. (1992). A thermosphere/ionosphere general circulation model with coupled electrodynamics. *Geophysical Research Letters*, *19*(6), 601–604. https://doi.org/10.1029/92GL00401

Rong, Z. J., Lui, A. T. Y., Wan, W. X., Yang, Y. Y., Shen, C., Petrukovich, A. A., et al. (2015). Time delay of interplanetary magnetic field penetration into Earth's magnetotail. *Journal of Geophysical Research: Space Physics*, *120*(5), 3406–3414. https://doi.org/10.1002/2014JA020452

Ruohoniemi, J. M., & Greenwald, R. A. (1995). Observations of IMF and seasonal effects in high-latitude convection. *Geophysical Research Letters*, *22*(9), 1121–1124. https://doi.org/10.1029/95GL01066

Saita, S., Kadokura, A., Sato, N., Fujita, S., Tanaka, T., Ebihara, Y., et al. (2011). Displacement of conjugate points during a substorm in a global magnetohydrodynamic simulation. *Journal of Geophysical Research: Space Physics*, *116*(A6), A06213. https://doi.org/10.1029/2010JA016155

Sergeev, V. A., Pellinen, R. J., & Pulkkinen, T. I. (1996). Steady magnetospheric convection: A review of recent results. *Space Science Reviews*, *75*(3–4), 551–604. https://doi.org/10.1007/bf00833344

Siscoe, G. L., & Huang, T. S. (1985). Polar cap inflation and deflation. *Journal of Geophysical Research: Space Physics*, *90*(A1), 543–547. https://doi.org/10.1029/JA090iA01p00543

Stenbaek-Nielsen, H. C., & Otto, A. (1997). Conjugate auroras and the interplanetary magnetic field. *Journal of Geophysical Research: Space Physics*, *102*(A2), 2223–2232. https://doi.org/10.1029/96JA03563

Tenfjord, P., Østgaard, N., Haaland, S. E., Snekvik, K., Laundal, K. M., Reistad, J. P., & Ohma, A. (2018). How the IMF B_y induces a local B_y component during northward IMF B_z and characteristic timescales. *Journal of Geophysical Research: Space Physics*, *123*(5), 3333–3348. https://doi.org/10.1002/2018JA025186

Tenfjord, P., Østgaard, N., Snekvik, K., Laundal, K. M., Reistad, J. P., Haaland, S. E., et al. (2015). How the IMF B_y induces a B_y component in the closed magnetosphere and how it leads to asymmetric currents and convection patterns in the two hemispheres. *Journal of Geophysical Research: Space Physics*, *120*(11), 9368–9384. https://doi.org/10.1002/2015JA021579

Tenfjord, P., Østgaard, N., Strangeway, R., Haaland, S. E., Snekvik, K., Laundal, K. M., et al. (2017). Magnetospheric response and reconfiguration times following IMF B_y reversals. *Journal of Geophysical Research: Space Physics*, *122*(1), 417–431. https://doi.org/10.1002/2016JA023018

Thomas, E. G., & Shepherd, S. G. (2018). Statistical patterns of ionospheric convection derived from mid-latitude, high-latitude, and polar SuperDARN HF radar observations. *Journal of Geophysical Research: Space Physics*, *123*(4), 3196–3216. https://doi.org/10.1002/2018JA025280

Tsyganenko, N. A., & Fairfield, D. H. (2004). Global shape of the magnetotail current sheet as derived from geotail and polar data. *Journal of Geophysical Research: Space Physics*, *109*(A3), A03218. https://doi.org/10.1029/2003JA010062

Wang, H., Lühr, H., Ma, S. Y., & Frey, H. U. (2007). Interhemispheric comparison of average substorm onset locations: Evidence for deviation from conjugacy. *Annales Geophysicae*, *25*(4), 989–999. https://doi.org/10.5194/angeo-25-989-2007

Weimer, D. R. (1995). Models of high-latitude electric potentials derived with a least error fit of spherical harmonic coefficients. *Journal of Geophysical Research: Space Physics*, *100*(A10), 19595–19607. https://doi.org/10.1029/95JA01755

Wild, J. A., Woodfield, E. E., & Morley, S. K. (2009). On the triggering of auroral substorms by northward turnings of the interplanetary magnetic field. *Annales Geophysicae*, *27*(9), 3559–3570. https://doi.org/10.5194/angeo-27-3559-2009

Wing, S., Newell, P. T., Sibeck, D. G., & Baker, K. B. (1995). A large statistical study of the entry of interplanetary magnetic field Y-component into the magnetosphere. *Geophysical Research Letters*, *22*(16), 2083–2086. https://doi.org/10.1029/95GL02261

Yamaguchi, R., Kawano, H., Ohtani, S., Kokubun, S., & Yumoto, K. (2004). Total pressure variations in the magnetotail as a function of the position and the substorm magnitude. *Journal of Geophysical Research: Space Physics*, *109*(A3), A03206. https://doi.org/10.1029/2003JA010196